Title: High-Resolution Methane Detection with the GHGSat Constellation

Authors: Antoine Ramier, Marianne Girard, Dylan Jervis, Jean-Philippe MacLean, David Marshall, Jason McKeever, Mathias Strupler, Ewan Tarrant, David Young

High-Resolution Methane Detection with the GHGSat Constellation

Antoine Ramier[a]*, Marianne Girard[a], Dylan Jervis[a], Jean-Philippe MacLean[a], David Marshall[a], Jason McKeever[a], Mathias Strupler[a], Ewan Tarrant[a], David Young[a]

[a] *GHGSat Inc., 1130 rue Sherbrooke Ouest, Montréal, Québec,Canada** Corresponding Author, aramier@ghgsat.com

Abstract

GHGSat operates a constellation of small satellites designed to detect and quantify methane emissions with high sensitivity compared with existing satellite technologies. An important feature of GHGSat measurements is the high spatial resolution (~25m), which enables attribution of emissions to specific facilities and subsequent corrective action from the operator. The GHGSat constellation currently has 9 satellites in orbit, and 3 more are planned for launch before the end of 2023 which will enable up to daily revisit times for any site in the world. This proceeding provides an overview of the GHGSat instruments, constellation, and processing algorithms. We also evaluate key instrument performance metrics, including column precision, detection threshold and quantification accuracy.

Keywords

Methane, Remote Sensing, Satellite

Acronyms/Abbreviations

GHG: Greenhouse gas

SWIR: Shortwave Infrared

IME: Integrated Mass Enhancement

LES: Large Eddy Simulations

PoD: Probability of Detection

1. Introduction

Methane is a potent greenhouse gas (GHG) which accounts for about 20% of global warming since pre-industrial era, second only to carbon dioxide [1]. Because of its relatively short lifetime in the atmosphere, reducing methane emissions is one of the most effective ways to fight climate change in the short and medium terms.

Anthropogenic methane emissions are mainly caused by agriculture, the fossil fuel industry, and waste management. It is estimated that methane emissions must be reduced by 34% before 2030 to comply with

the Paris agreement and limit the global temperature rise below 1.5 °C [2]. Curbing down emissions at this rate is a significant endeavour that will require a wide and concerted set of measures. A critical piece of this ensemble is the capability to detect and monitor methane emissions, particularly unintentional, fugitive emissions.

Satellite-based remote sensing is a well-established technology to survey atmospheric composition, including greenhouse gases. Instruments such as GOSAT and TROPOMI have provided global-scale measurements that are essential for studying and modelling the Earth climate. However, those sensors are not well suited to identifying individual sources of methane and can only detect the largest among them.

GHGSat has pioneered the development of satellites that are designed specifically for detecting methane point sources. Its first demonstration satellite, GHGSat-D (Claire) was launched in 2016, followed-up by a series of commercial payloads with greatly improved performance. The GHGSat constellation now consists of 9 microsatellites in orbit, and 3 more are planned for launch in the coming year. The spacecrafts are about 40×30×20 cm^3 in size and 15 kg in weight, and are in polar sun-synchronous orbit. Two important features of GHGSat measurements are:

1. High precision methane measurements (1.4-2.9 % of background) to detect relatively small sources (>100 kg/hr)
2. High spatial resolution (~25 m), which enables attribution of emissions to specific facilities and subsequent corrective action from the operator.

This proceeding presents an overview of the GHGSat constellation, payload design and data processing algorithms. We also show the results of calibration and validation experiments and use them to assess the instruments' performance in terms of column precision, source detection sensitivity, and emission rate quantification accuracy.

2. Technology

Remote methane sensing by GHGSat and other satellites is based on the technique of differential absorption spectroscopy. Briefly, sunlight traverses the atmosphere, is partially reflected by the earth surface, and travels back up to the satellite. Gas molecules absorb some of the electromagnetic wave, at wavelengths that are characteristic of molecular species. Gas concentration is inferred by measuring how much light is missing at those wavelengths compared to a reference atmosphere. GHGSat instruments use the methane absorption lines around 1.65 µm, in the shortwave infrared (SWIR) band. The imaging spectrometer is based on a wide-angle Fabry-Pérot (WAF-P) interferometer. A detailed presentation of the payload optical design and measurement strategy is available in ref. [3].

Inherent to this core sensing methodology is a compromise between 3 key performance parameters: spatial resolution, precision, and coverage. To detect methane sources with minimal emission rate, a fine spatial resolution and a precise measurement are required [4]. The appropriate balance of specifications is a mission-specific design choice, but some broad categories of instruments are commonly encountered.

Instruments with high coverage and precision, such as TROPOMI, are sometimes referred to as area flux mappers [5], because their measurements can be used to infer gas fluxes on global or regional scales. They are less sensitive to methane point sources because the large pixels effectively dilute the points of highest methane concentrations that are found next to the source.

Multispectral imagers such as Landsat-8/9 and Sentinel-2 have good resolution and coverage but use a few wide spectral bands that cannot resolve the fine spectral features of methane and thus limit precision.

Instruments with high resolution and precision provide the best sensitivity to methane point sources at the expense of a smaller field of view. GHGSat satellites are the only methane-sensing satellites currently in operation that fall into that category. The upcoming Carbon Mapper is another example.

Because of the compromise on spatiotemporal coverage, GHGSat satellites do not image the whole planet on a regular basis. Instead, they are operated in target mode, focusing on specific regions that contain facilities of interests. A typical targeted observation covers 40×12 km², or 15×12 km² for isolated facilities.

Tip-and-cue using publicly available data from other satellites is also used to identify sites with high probability of emissions [6]. In addition, since GHGSat's satellites are small and cost-effective, a larger number can be deployed to improve coverage. A revisit opportunity time of 1 or 2 days can be achieved with the 9 satellites currently on orbit, weather permitting.

2.1. Methane column density retrievals

The amount of methane above background level is obtained by nonlinear regression. A numerical model describes the light propagation through the atmosphere and instrument and predicts how much irradiance is sensed at the instrument's focal plane array (SWIR camera). Nonlinear optimization is used to infer the model inputs or state vector (methane concentration and ground reflectance) that best explains the measured data.

Because of the computational cost of evaluating full-physics radiative transfer models at every ground cell, the retrieval is broken down into 2 steps:

1. Full-physics retrieval on scene-wide averaged signal, in which instrument parameters and average methane concentration are retrieved.
2. The forward model is partially linearized, using the values from step 1 as the reference for Taylor expansion. Then, a regression is computed for every ground cell based on this model, to retrieve the methane column density and parameters of a reflectance model.

Methane emissions correspond to regions where the retrieved column density is higher than the background value, as illustrated in Fig. 1. The source of the emission can be localized at the origin of the plume. The retrieved reflectance, combined with information from the satellite attitude control module, is used to geographically reference the observations, such that emissions can be attributed to specific facilities.

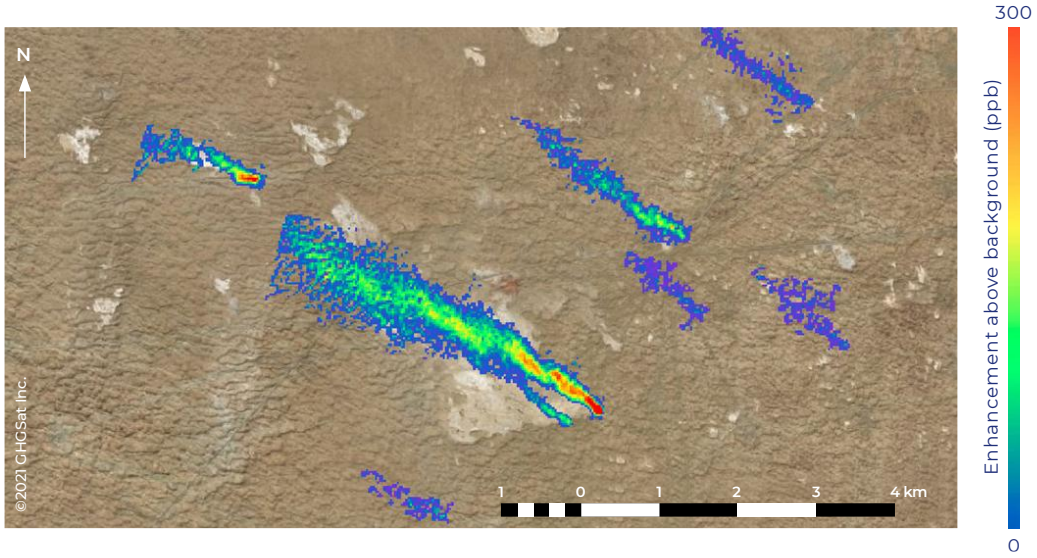

Fig. 1. Multiple methane emissions observed by a GHGSat satellite in an oil and gas field in central Asia. Methane concentration enhancement above background level is shown in pseudocolour, overlaid on top of standard imagery provided by Bing Maps.

2.2. Source rate quantification

The retrieval algorithm described above produces a map of methane column density at a given time, which allows to detect emissions, but does not immediately tell the rate at which methane is emitted. How much methane is visible (above the noise level) depends on two critical factors: the emission rate Q, and the time τ this gas stays in the visible plume before dissipating in the surrounding atmosphere. The dissipation time is largely driven by wind speed U. This relationship is the basis of the Integrated Mass Enhancement (IME) method [7], which is used by GHGSat to quantify emission rates.

The initial step of this method is to define a plume mask, which specifies in which cell the methane enhancement is higher than the measurement uncertainty. The emission rate is then given by the equation

$$Q = \frac{\mathrm{IME}}{\tau} = \frac{U_{\mathrm{eff}}}{\sqrt{A}}\,\mathrm{IME} \qquad (1)$$

where U_{eff} is the effective wind speed, A is the area of the plume mask, and IME is the total mass of methane within the mask. The concept of effective wind speed is introduced because methane dissipation depends not only on the average wind speed, but also on the small-scale atmospheric turbulence. This parameter was calibrated as a function of the standard 10-meter wind speed (U_{10}) using large eddy simulations (LES) to obtain a relationship that is valid over a wide range of possible plume realizations and atmospheric conditions [7].

3. Performance quantification

This section presents the results of calibration and validation experiments that were conducted to assess the performance of the GHGSat satellite instruments. Three specific aspects are discussed: (1) column precision, which is the uncertainty of the retrieved column density, (2) detection sensitivity (3) quantification accuracy.

3.1. Column precision

Methane column density is the main output of the retrieval algorithm. Its associated uncertainty, column precision, is therefore an important performance metric and a key driver of the ability to detect small emissions.

There are multiple ways to estimate column precision. It can be predicted from theory based on the amount of light collected (shot noise) and camera specifications (readout noise) or estimated from the fit residuals. Those approaches are useful for design and analysis but can underestimate the impact of artifacts and unmodeled physical effects.

A more empirical way to estimate the column precision is to measure the spatial standard deviation within a region of interest of the retrieval domain, in areas where there are no actual methane emissions. Because we retrieve methane enhancements above background level, the value should be zero, and any variability reflects the uncertainty of retrieved methane. The window within which the noise statistics are computed is a square of 500 × 500 m², a scale relevant for small methane plume detection. Cells that are quality-flagged (e.g. cloud-covered or over water bodies) are excluded from the analysis.

Note that the column precision is not constant from observation to observation or even over the domain of a single retrieval. It depends on factors such as the ground reflectance and the angles that define the sun-ground-satellite observation geometry. We therefore collect the distribution of column precisions by sliding the window across the full retrieval domain and repeat this process over a large sample of observations.

The analysis presented here includes all successful observations over a 1-year period (5700 observations taken between November 2021 and 2022) for the satellites GHGSat-C2 to GHGSat-C5. Results from this retrospective are plotted in Fig. 2 below. The median column precision is 2% of the background CH4 atmospheric concentration (650 mmol/m²), and the interquartile range is 1.4% to 2.9%.

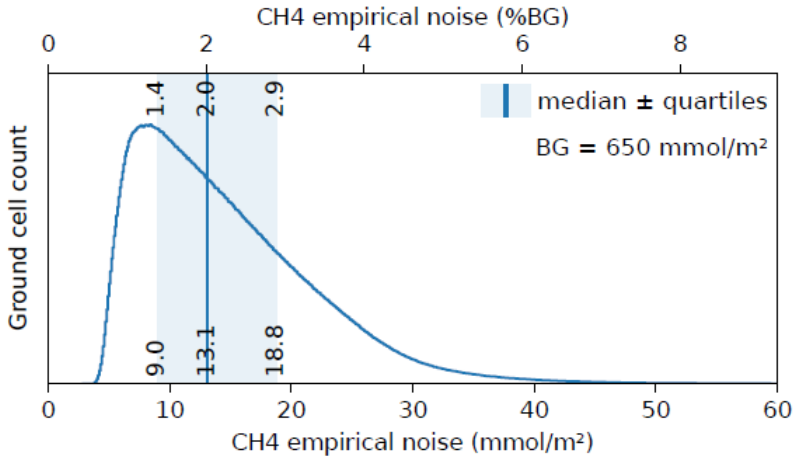

Fig. 2. Distribution of empirically measured methane precision. The x-axis is expressed in two different units: as a column density enhancement (mmol/m²) at the bottom, and as a percentage of the background (650 mmol/m²) on top.

As mentioned earlier, the precision is expected to depend on ground reflectance, which defines the amount of shot noise in the raw signal. Fig. 3-a shows the joint distribution between those two variables, highlighting the fact that the methane uncertainty is lower over bright, reflective ground, and higher over signal-starved darker regions.

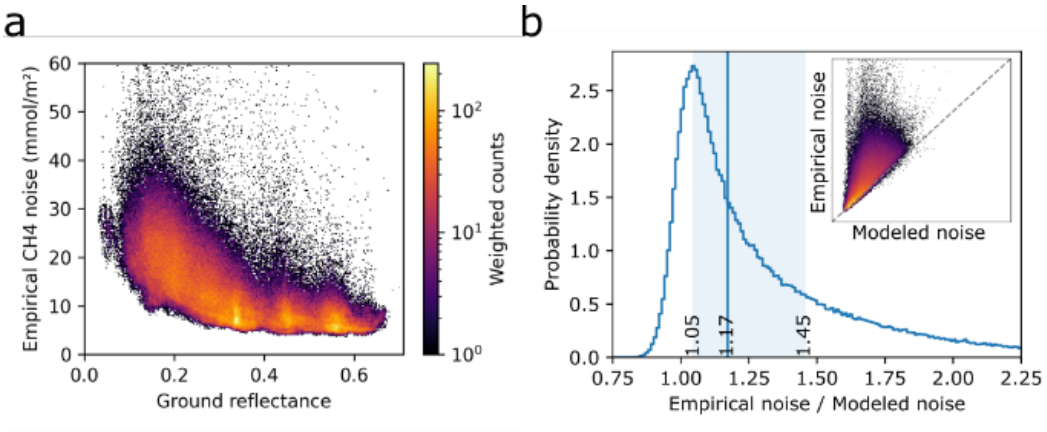

Fig. 3. Factors driving the column precision. (a) Joint distribution of empirical precision as a function of ground reflectance. (b) Histogram of the ratio between empirical noise and a model based on shot and readout noise. The shaded region and vertical line represent the 25th and 75th percentiles and the median. The inset shows the same data as a joint distribution with logarithmic color scale.

The contribution of shot noise to the methane-sensing precision can be modelled explicitly, providing a "best-case" noise estimate. This modelled noise is compared with the empirical noise in Fig. 3-b, which plots the ratio of the empirical / modelled precision estimates as a histogram. Additionally, an inset shows the direct relationship between the two noise metrics.

We see that most of the empirical precision lies close but above the theoretical model: within 17% of the shot noise limit for 50% of the surveyed area (within 45% for 75% of the surveyed area).

This analysis suggests that the spread of possible precisions is largely driven by variations in ground reflectance and provide an estimate for the magnitude of additional contributions from unmodeled sources.

3.2. Sensitivity and detection limit

Detection limit, also known as detection threshold, is a key specification for end users of the satellite detection service. It is the smallest methane emission rate that can be detected by the observing system with a given level of confidence. This metric is closely related to the concept of sensitivity, which is the probability that a methane emission will be successfully detected when observed by the satellite.

The probability of detection (PoD) is not a constant for a given system. It depends mainly on

- *Emission rate*: large sources are easier to detect than small ones.
- *Wind speed (dispersion rate)*: strong winds rapidly disperse the emitted methane in the surrounding atmosphere, which accumulates in lower concentrations that are harder to detect.

- *Column precision*: detection ultimately depends on the signal to noise ratio. While emission and dispersion rate determine the signal, column precision is the background noise above which this signal must rise to be detectable. For a given system, precision is affected by external conditions such as ground reflectance: more signal is collected over bright, reflective ground, resulting in more precise column density retrievals.

To enable comparisons between different detection systems, PoD can be expressed as a function of emission rate and wind speed, and should be tested in the same or equivalent conditions. Alternatively, when a single figure of merit is required, the detection threshold can be specified at a standard PoD (for example 50% or 90% probability) and wind speed (typically 3 m/s).

A well established approach to quantify the probability of detection for an instrument is through controlled release experiments: a known flow rate of methane (possibly zero) is intentionally released in the atmosphere while the satellite scans the area. This is repeated for multiple flow rates over the expected dynamic range of the instrument. Wind conditions are measured on site to avoid the large uncertainties associated with wind fields in weather models.

Results from controlled release experiments through 2024 are shown in Fig. 4. Each marker represents an individual controlled release event. The results are then fit to a probability of detection model [8] based a log-normal distribution:

$$p(Q, U\,; U_0, \sigma, \mu) = \frac{1}{2}\left(1 + \mathrm{erf}\left(\frac{\ln g(Q, U; U_0) - \mu}{\sigma}\right)\right) \tag{2}$$

$$g(Q, U; U_0) = \frac{Q}{U - U_0} \tag{3}$$

where p is the detection probability, erf is the error function, Q is the emission rate, and U is the wind speed, μ and σ are the parameters of the lognormal distribution, and U_0 is a wind speed offset which accounts for the presence of some amount of dispersion even at zero wind speed. The parameters U_0, μ and σ are fitted to the controlled release data.

The detection threshold at "standard" wind speed and probability level can be extracted by isolating Q in this expression. We find that the emission rate of 100 kg/hr at 3 m/s wind speed is detectable with 50% probability [9].

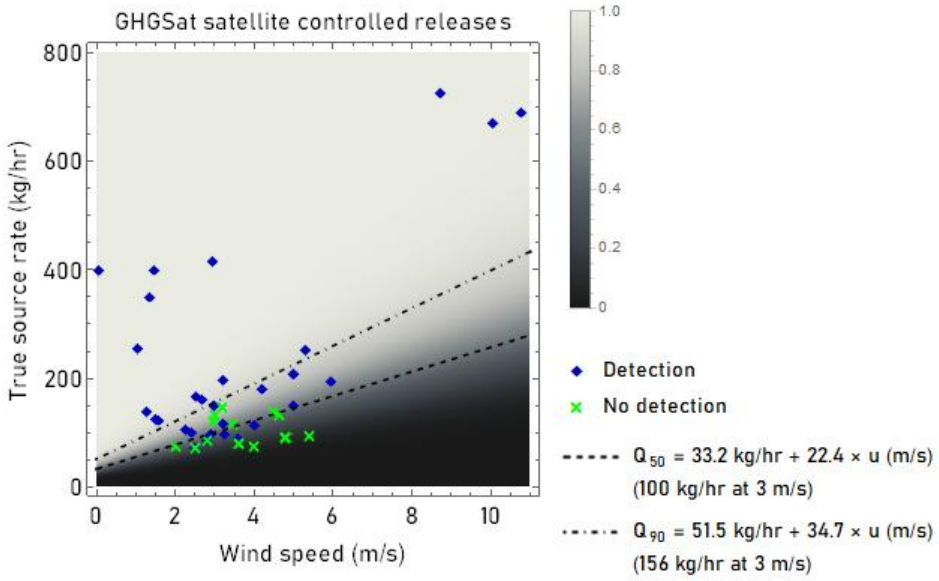

Fig. 4. Methane probability of detection for the GHGSat satellite instruments. Blue diamonds are successful detections and green crosses are missed plumes. The background heatmap (black to white) is the fitted probability of detection model, and the dashed lines represents the 50% and 90% probability detection thresholds as a function of wind speed.

For an unbiased quantification of the detection threshold, the measurement provider should be "blind" to the actions of the ground team (does not know if methane is emitted or not, and the exact location). GHGSat has participated in controlled release campaigns organized by independent third-parties [10]. The number of samples in the first phase of this study is insufficient to quantify the detection threshold (all emissions were large enough to be detected). The data shown in Fig. 4 therefore also includes results from internally organized releases. The number of samples will be increased in future studies.

3.3. Quantification accuracy

In addition to detection sensitivity, third-party, single-blind controlled releases are used to assess quantification accuracy, by comparing the source rate computed by the measurement provider (GHGSat) with the "ground truth" flow rate. A detailed description of the methodology and equipment is available in ref. [10]. This comparison is plotted in Fig. 5.

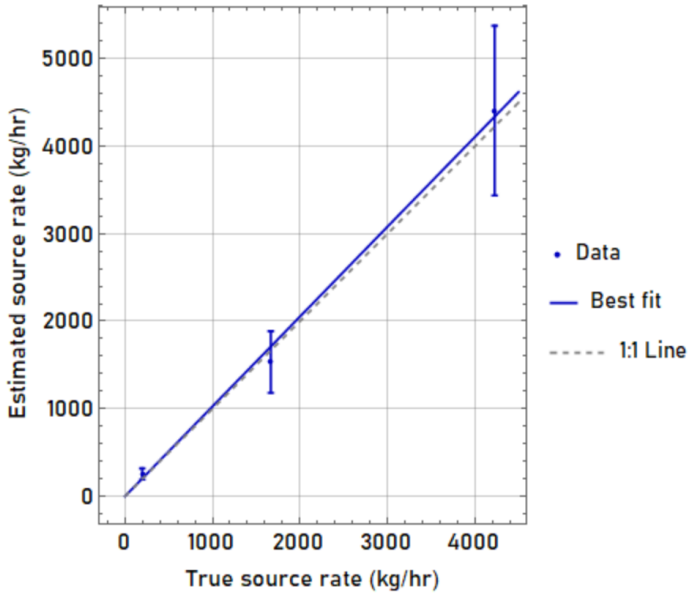

Fig. 5. Source rate quantification accuracy.

At this point, the results show no evidence of a significant nonlinearity or bias. The best fit line deviates from unity by 2.7 %. This suggests that the quantification error is dominated by the random component associated with the measurement uncertainty (error bars).

4. Conclusion

The measurements and analysis presented in this proceeding show that the GHGSat methane-sensing satellites have a median column precision of 2 % of the atmospheric background. The limit of detection for individual emissions, measured in controlled releases, is 100 kg/hr at 3 m/s wind and 50 % PoD.

As a concluding remark, an effective observing system takes advantage of complementarity between different methane detection technologies. Those include ground-based surveys, remote-sensing from aircraft or drones, and satellites optimized for different temporal, spatial, and spectral scales. GHGSat provides aircraft-based methane monitoring, based on the same technology as the satellites. The finer spatial resolution available at shorter range allows for a lower limit of detection than satellites, at the expense of a smaller field of view. At the other end of the spectrum, GHGSat offers global survey services based on third party data from public satellites such as TROPOMI and Sentinel-2 [6], [11] to rapidly identify large emissions, and to suggest candidate targets for follow-up measurements.

5. References

[1] Intergovernmental Panel On Climate Change (Ipcc), *Climate Change 2021 – The Physical Science Basis: Working Group I Contribution to the Sixth Assessment Report of the Intergovernmental Panel on Climate Change*, 1st ed. Cambridge University Press, 2023. doi: 10.1017/9781009157896.

[2] Intergovernmental Panel On Climate Change (Ipcc), Ed., *Climate Change 2022 - Mitigation of Climate Change: Working Group III Contribution to the Sixth Assessment Report of the Intergovernmental Panel on Climate Change*, 1st ed. Cambridge University Press, 2023. doi: 10.1017/9781009157926.

[3] D. Jervis *et al.*, 'The GHGSat-D imaging spectrometer', *Atmos. Meas. Tech.*, vol. 14, no. 3, pp. 2127–2140, Mar. 2021, doi: 10.5194/amt-14-2127-2021.

[4] T. Hill and R. Nassar, 'Pixel Size and Revisit Rate Requirements for Monitoring Power Plant CO2 Emissions from Space', *Remote Sensing*, vol. 11, no. 13, p. 1608, Jul. 2019, doi: 10.3390/rs11131608.

[5] D. J. Jacob *et al.*, 'Quantifying methane emissions from the global scale down to point sources using satellite observations of atmospheric methane', *Atmos. Chem. Phys.*, vol. 22, no. 14, pp. 9617–9646, Jul. 2022, doi: 10.5194/acp-22-9617-2022.

[6] J. D. Maasakkers *et al.*, 'Using satellites to uncover large methane emissions from landfills', *Sci. Adv.*, vol. 8, no. 32, p. eabn9683, Aug. 2022, doi: 10.1126/sciadv.abn9683.

[7] D. J. Varon *et al.*, 'Quantifying methane point sources from fine-scale satellite observations of atmospheric methane plumes', *Atmos. Meas. Tech.*, vol. 11, no. 10, pp. 5673–5686, Oct. 2018, doi: 10.5194/amt-11-5673-2018.

[8] B. M. Conrad, D. R. Tyner, and M. R. Johnson, 'Robust probabilities of detection and quantification uncertainty for aerial methane detection: Examples for three airborne technologies', *Remote Sensing of Environment*, vol. 288, p. 113499, Apr. 2023, doi: 10.1016/j.rse.2023.113499.

[9] J. McKeever and D. Jervis, 'Validation and Metrics for Emissions Detection by Satellite', GHGSat Inc., White Paper, Sep. 2022. [Online]. Available: https://go.ghgsat.com/hubfs/Reports/WhitePaper_Validation%20and%20Metrics%20for%20Emissions%20Detection%20by%20Satellite_JMcKeeverDJervis_092022.pdf

[10] E. D. Sherwin *et al.*, 'Single-blind validation of space-based point-source detection and quantification of onshore methane emissions', *Sci Rep*, vol. 13, no. 1, p. 3836, Mar. 2023, doi: 10.1038/s41598-023-30761-2.

[11] D. J. Varon, D. Jervis, J. McKeever, I. Spence, D. Gains, and D. J. Jacob, 'High-frequency monitoring of anomalous methane point sources with multispectral Sentinel-2 satellite observations', *Atmos. Meas. Tech.*, vol. 14, no. 4, pp. 2771–2785, Apr. 2021, doi: 10.5194/amt-14-2771-2021.